Geophysical Research Letters

RESEARCH LETTER
10.1029/2020GL088350

Key Points:
- Transport time series of the Atlantic North Equatorial Undercurrent are estimated from moored observations
- North Equatorial Undercurrent is dominated by intraseasonal variability, only a weak seasonal cycle is observed
- Eastward oxygen supply by North Equatorial Undercurrent increases occasionally due to short sporadic events

Supporting Information:
- Supporting Information S1

Correspondence to:
K. Burmeister,
kristin.burmeister@sams.ac.uk

Citation:
Burmeister, K., Luebbecke, J. F., Brandt, P., Claus, M., & Hahn, J. (2020). Fluctuations of the Atlantic North Equatorial Undercurrent and associated changes in oxygen transports. *Geophysical Research Letters*, *47*, e2020GL088350. https://doi.org/10.1029/2020GL088350

Received 15 APR 2020
Accepted 1 JUN 2020
Accepted article online 9 JUN 2020

Fluctuations of the Atlantic North Equatorial Undercurrent and Associated Changes in Oxygen Transports

Kristin Burmeister[1,2], Joke F. Luebbecke[1,3], Peter Brandt[1,3], Martin Claus[1,3], and Johannes Hahn[1]

[1]GEOMAR Helmholtz Centre for Ocean Research Kiel, Kiel, Germany, [2]Now at SAMS, Scottish Association for Marine Science, Oban, UK, [3]Christian-Albrechts-Universität zu Kiel, Kiel, Germany

Abstract Although the core velocity of the Atlantic North Equatorial Undercurrent (NEUC) is low (0.1–0.3 m s^{-1}), it has been suggested to act as an important oxygen supply route towards the oxygen minimum zone in the eastern tropical North Atlantic. For the first time, the intraseasonal to interannual NEUC variability and its impact on oxygen are investigated based on shipboard and moored velocity observations around 5°N, 23°W. In contrast to previous studies that were mainly based on models or hydrographic data, we find hardly any seasonal cycle of NEUC transports in the central Atlantic. The NEUC transport variability is instead dominated by sporadic intraseasonal events. Only some of these events are associated with high oxygen levels suggesting an occasional eastward oxygen supply by NEUC transport events. Nevertheless, they likely contribute to the local oxygen maximum in the mean shipboard section along 23°W at the NEUC core position.

Plain Language Summary In the eastern tropical North Atlantic, a zone of low-oxygen waters exists between 100 and 700 m depth due to high oxygen consumption and weak exchange of water masses. Long-term oxygen changes in this zone have been reported with possible impacts on, for example, the ecosystem or the available habitat for fish. Typically, water masses in that region are exchanged via weak eastward and westward currents. As the oxygen concentration in the western Atlantic basin is high, an eastward current such as the North Equatorial Undercurrent (NEUC) may transport oxygen-rich waters into the eastern low-oxygen zone. Given the east-west difference in oxygen concentration, we assume that a stronger NEUC is transporting more oxygen-rich water from the western towards the eastern basin. This is the first study that investigates the variations in NEUC transport based on direct velocity measurements at 5°N, 23°W. In contrast to previous studies based on model simulations or hydrographic data, we do not find a seasonal cycle of the NEUC transport. Instead, changes of the NEUC transport are dominated by bursts of eastward flow which persist for a few months. These eastward flow bursts are only occasionally associated with higher oxygen concentrations.

1. Introduction

The circulation of the upper tropical Atlantic Ocean is characterized by a complex current system which takes part in the wind-driven equatorial gyre circulation, the shallow subtropical and tropical overturning cells and the basin-wide Atlantic meridional overturning circulation (e.g., Hazeleger & Drijfhout, 2006; Schott et al., 2004). Zonal currents play a key role in the basin wide distribution of water mass properties and affect the transport of heat, salt, and biogeochemical components such as oxygen (e.g., Brandt et al., 2015; Hazeleger & Drijfhout, 2006; Schott et al., 2004). The North Equatorial Undercurrent (NEUC) is an eastward flowing subsurface (here defined in the depth range 65–270 m) current centered at 5°N. Its upper limit is commonly defined as the 24.5 kg m^{-3} neutral density layer, which separates the tropical surface water from the subtropical underwater (e.g., Bourlès et al., 1999; Goes et al., 2013; Schott et al., 1995). Although the NEUC core velocity (0.1 to 0.3 m s^{-1}) is one of the lowest among the wind-driven off-equatorial currents in the tropical Atlantic, the NEUC has been suggested to act as an important oxygen supply route towards the Oxygen Minimum Zone (OMZ) in the Eastern Tropical North Atlantic (Brandt et al., 2010; Stramma et al., 2008). Hahn et al. (2017) observed a shoaling of the Eastern Tropical North Atlantic OMZ since 2006 which is associated with a thinning of the available habitat of tropical pelagic fishes (Stramma

et al., 2012). The intraseasonal to interannual variability of the NEUC causes oxygen variability along the OMZ boundary. Under global warming with increasing mean oxygen gradients, oxygen variance might enhance the impact on tropical pelagic ecosystems and biogeochemical cycles.

Model studies generally agree that the NEUC is mainly in geostrophic balance, but its driving mechanism is under discussion. Potential mechanisms that were described for the NEUC or similar subsurface currents in other tropical basins are the conservation of angular momentum of the tropical overturning cells (Marin et al., 2000), the Eliassen–Palm flux associated with the propagation of Tropical Instability Waves (TIWs Jochum & Malanotte-Rizzoli, 2004) or the pull of upwelling within domes in the eastern basin or at the eastern boundary (Furue et al., 2007, 2009; McCreary et al., 2002).

Until now, the seasonal to long-term variability of the NEUC has been investigated based on model output (Burmeister et al., 2019; Hüttl-Kabus & Böning, 2008) or geostrophic velocities derived from a combination of hydrography and satellite data (Goes et al., 2013). In these studies, a seasonal cycle of the NEUC with amplitudes of 1 to 3.5 Sv was identified. In general, NEUC transport estimates derived from meridional ship sections are obscured by mesoscale activity (Weisberg & Weingartner, 1988) and interannual variability (Hüttl-Kabus & Böning, 2008). So far, studies based on shipboard velocity observations have not been able to detect a seasonal cycle of the NEUC (Bourlès et al., 1999, 2002; Burmeister et al., 2019; Schott et al., 1995, 2003; Urbano et al., 2008).

For the first time, we will investigate the NEUC variability using direct velocity observations. In this study we reconstruct the eastward transport associated with the NEUC at 5°N, 23°W using moored velocity observations from June 2006 to February 2008 and November 2009 to January 2018 in combination with 24 meridional ship sections taken between 21°W and 26°W. This study aims to investigate the intraseasonal to interannual variability of the NEUC and its impact on oxygen levels.

2. Data

Moored Acoustic Doppler Current Profiler (ADCP) velocity, hydrography, and oxygen data are available at 5°N, 23°W (June 2006 to February 2008, November 2009 to January 2018) as well as at 4.6°N, 22.4°W and 4.5°N, 23.4°W (November 2012 to April 2014). All instruments were set to a sampling rate of 2 h or higher. The upper limit of the ADCP observations varies between 65 and 85 m, the lower limit is at least 755 m. The moored velocity data were linearly interpolated onto a regular time-depth grid (12 h × 10 m), and a 40-day low-pass Butterworth filter was applied to remove tides from the time series. As the NEUC is located approximately between 3.5°N and 6°N and in a depth of about 65 to 270 m at 23°W (Burmeister et al., 2019), the moored velocity observations do not always cover the entire extent of the NEUC which can result in an underestimation of its mean transport. Observations of dissolved oxygen, temperature, conductivity, and pressure were used from respective sensors that were installed at the mooring at 5°N, 23°W in 100, 200, and 300 m depth. The moored hydrography and oxygen data were interpolated onto a 12-h time grid. This data set is an extension of the one used in Hahn et al. (2014, see supporting information Text S1 for more details).

In addition to the mooring time series, we use data from 24 meridional ship sections taken between 21°W and 26°W in the time period 2002 to 2018 (supporting information, Table S1). Only shipboard ADCP (Fischer et al., 2003), hydrography and oxygen sections that cover at least the upper 350 m between 0° and 10°N are used. The ship sections are an extension of the data set used in Burmeister (2019, see Text S1 for more details).

3. Observed Velocity Variability at 5°N, 23°W

Moored ADCP measurements at 5°N, 23°W show a weak mean eastward velocity with maximum values of 9 cm s^{-1} at the upper limit of the ADCP range (85 m), while the meridional velocity varies around zero (Figures 1a and 1b). In the upper limit (300 m), zonal and meridional velocities exhibit anomalies of comparable magnitude. The periodogram of the horizontal velocity components indicates variability over a range of frequencies, in particular in the intraseasonal band (Figure 1c). While the zonal velocity exhibits variability mainly for periods greater than 70 days, the meridional velocity is dominated by variability with periods between 35 and 75 days which is associated with TIWs (Jochum & Malanotte-Rizzoli, 2003). The zonal

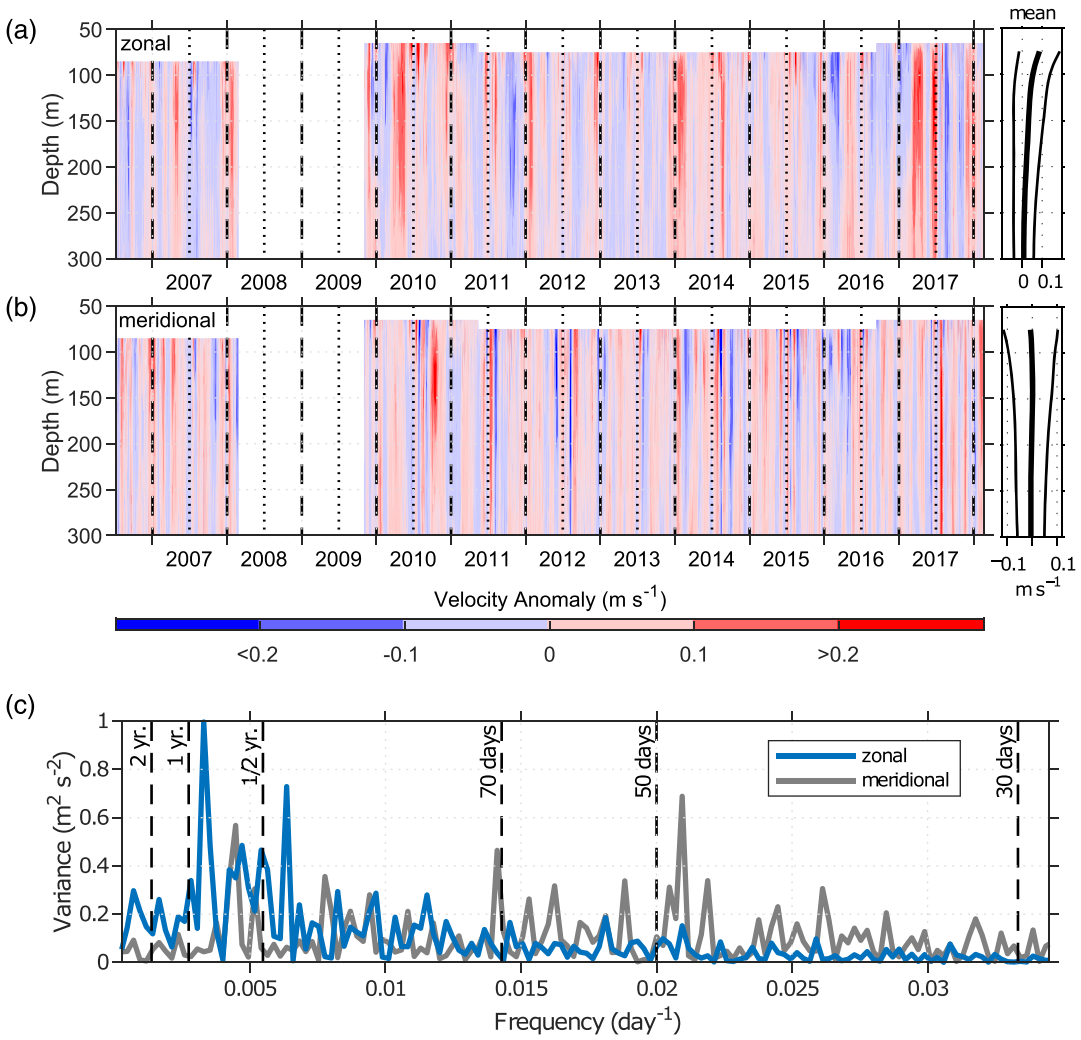

Figure 1. Anomalous (a) zonal and (b) meridional velocity measurements from moored ADCPs at 5°N, 23°W. The temporal mean profiles (thick black line) are shown at the right side of the (a) zonal and (b) meridional velocity time series. The thin black line marks the mean profile ± one standard deviation. (c) Lomb–Scargle periodogram of zonal (blue line) and meridional (grey line) velocity averaged between 95 and 275 m depth.

velocity, while eastward in the mean, occasionally changes to westward. Its variability is characterized by strong eastward anomalies with a duration of about 1 to 5 months occurring without a clear seasonal preference. Unexpectedly, the seasonal cycle of the zonal velocity is much weaker than found in previous studies (Burmeister et al., 2019; Goes et al., 2013; Hüttl-Kabus & Böning, 2008). The annual harmonic fit with a maximum amplitude of 3 cm s^{-1} only explains between 2% (85 m) and 9% (300 m) of the zonal velocity variability. For the semi-annual harmonic fit, we derived a maximum amplitude of 5 cm s^{-1} and an explained variance between 11% (75 m) and 1% (300 m).

4. NEUC Transport Estimates at 23°W

In this study, the NEUC transport was estimated by four different methods using only eastward velocities. (i) We calculated the NEUC transport between the 24.5 and 26.8 kg m^{-3} neutral density surfaces from 24 ship sections using a path following algorithm developed by Hsin and Qiu (2012; Figure 2, green diamonds). This method follows the current core, thereby avoiding artifacts in the transport calculation if the current is meridionally migrating (see supporting information Text S2 for more details). Using this method, we estimate a mean NEUC transport of 2.7 ± 0.4 Sv. Uncertainties are given in terms of the standard error. In the following, we consider this estimate as a reference NEUC transport keeping in mind that the NEUC transport

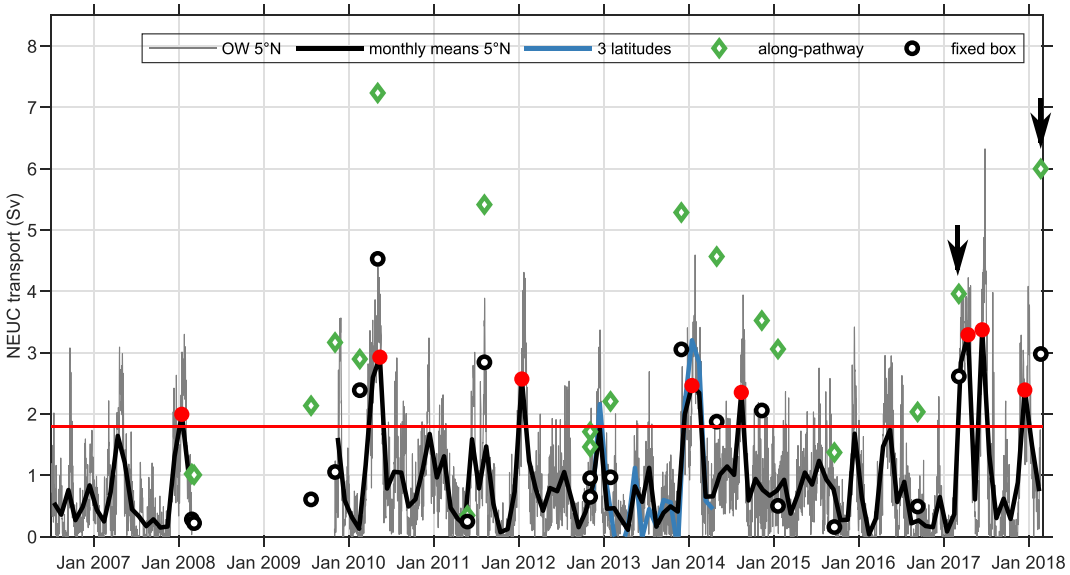

Figure 2. NEUC transport at 23°W calculated by four different methods: (i) from ship observations using a path following algorithm (green diamonds); (ii) from ship sections by integrating the eastward velocities in a fixed box (black circles); (iii) by the OW method combining ship sections and moored zonal velocities at three mooring positions (monthly means, blue line); (iv) by the OW method combining ship sections with moored zonal velocities at 5°N, 23°W (gray line). The black thick line shows the monthly mean values of the NEUC transport reconstructed at 5°N. The red line marks 2.5 times the standard deviation of the monthly mean transports used to define strong transport events (red dots). The black arrows mark the month of the cruises in 2017 and 2018.

estimate from ship sections can be obscured by mesoscale activity (Weisberg & Weingartner, 1988) and interannual variability (Hüttl-Kabus & Böning, 2008).

(ii) The second approach is also based on ship sections only, but with a fixed smaller integration box to be consistent with NEUC transports calculated from a combination of ship mounted and moored observations. We integrate the meridional sections of zonal velocity between 4.25°N and 5.25°N, 65 and 270 m (Figure 2, black circles). The mean fixed box integrated transport derived from ship sections is 1.4 ± 0.2 Sv. The fixed box integrated method underestimates the NEUC strength by 1.3 Sv. However, it represents the variability of the reference NEUC transport well (R=0.91, supporting information, Figure S2a).

(iii) We reconstruct the NEUC transport combining moored velocity observations at 5°N, 23°W as well as 4.6°N, 22.4°W and 4.5°N, 23.4°W and ship sections following the optimal width method described in Brandt et al. (2014). This method aims to find an optimal latitude range W_i for each mooring position i to reconstruct the latitudinally integrated zonal velocity $U(z,t)$ by

$$U(z,\,t) = \sum_{i=1}^{3} W_i u_i(z,\,t). \tag{1}$$

For this purpose, we latitudinally integrate the eastward velocities of each ship section from 4.25°N to 5.25°N. The latitudinally integrated velocity is then regressed onto the eastward velocities of the ship sections at the three mooring position between 65 and 270 m depth to obtain W_i. We estimated that the moorings at 5°N, 4.6°N, and 4.5°N correspond to latitude ranges, W_i, of 0.46°, 0.18°, and 0.37°, respectively. The NEUC transport is then reconstructed by integrating Equation 1 over the same depth range as for method (ii; Figure 2, blue line). Note that data from all three mooring positions are only available for the time period November 2012 to April 2014. The root mean square error of the reconstructed transport using method (iii) and the box integrated transport (method ii) using the shipboard data is 0.16 Sv. The mean reconstructed transport is 0.9 ± 0.3 Sv. For a validation of the method see supporting information, Text S2.

(iv) This method is similar to method (iii) but uses moored velocity observations only at 5°N, 23°W to obtain a longer transport time series (Figure 2 grey line). Here the 5°N mooring corresponds to a latitude range of 0.88°. Although the root mean square error between the reconstructed transport and the box integrated

transport increases (0.51 Sv) when using only one mooring, the reconstructed transport based on one mooring agrees well with the one reconstructed using three moorings (R=0.89). The mean NEUC transport is the same as estimated for method (iii), that is, 0.9 ± 0.2 Sv.

In the following, we will analyze the NEUC variability based on the reconstructed time series using only the mooring at 5°N, 23°W. Although the reconstructed transport time series from moored velocity observations tends to underestimate the mean current strength of the NEUC, we still consider the variability to be captured to a large extent. This is supported by transport estimates based on all three moorings combined with zonal velocity sections between 3.5°N and 6.0°N which agree reasonably well with the transport time series reconstructed by method (iii) accounting for velocities between 4.25°N and 5.25°N only (supporting information, Figures S2–S5, Text S2).

5. NEUC Variability

Similar to the zonal velocity, the NEUC transport is dominated by strong eastward anomalies that persist between 1 and 5 months. The transport time series do not exhibit a seasonal cycle. The explained variance of the annual and semi-annual harmonic is only 2% and 3%, respectively. We therefore focus the analysis on the intraseasonal eastward flow events. We define a strong eastward flow event rather arbitrary as the time period in which the NEUC transport exceeds 2.5 times the standard deviation of the complete monthly mean time series. We find eight such events which take about 1 to 5 months to develop, peak, and fade away (duration from local minimum to minimum in the transport time series). They have a maximum monthly mean transport between 2.3 and 3.8 Sv and peak without a clear seasonal preference (3 in January and 1 each in April, May, June, August, and December). During these events the 12-hourly transports reach maximum values from 3.8 to 7.2 Sv.

The NEUC at 5°N, 23°W appears to be rather weak, and it is likely that there are different generation mechanisms for the strong eastward flow events. The short period of intraseasonal events implies that the upwelling within the Guinea Dome in the eastern basin as suggested by McCreary et al. (2002) and Furue et al. (2007), Furue et al. (2009) may not be of first order in forcing them. To investigate the role of the wind forcing for the strong eastward flow events, we linearly regressed zonal wind stress anomalies (Bentamy & Fillon, 2012; Kobayashi et al., 2015; Large & Yeager, 2004) onto the NEUC transport time series (supporting information, Figure S6 and Text S3). Easterly wind stress anomalies in the eastern equatorial basin are leading the NEUC transports by 1 to 2 months. We hypothesize that these zonal wind stress anomalies may force equatorial Kelvin waves reflecting at the eastern boundary into westward propagating Rossby waves and poleward propagating coastal trapped waves. The northward propagating waves may shed Rossby waves when arriving at the exit of the Gulf of Guinea where the coastline turns northward. Such remotely forced Rossby waves may reach 5°N, 23°W, causing the observed eastward flow events. Rossby waves at 5°N, 23°W can also be forced locally by wind stress curl anomalies of small meridional scale (Burmeister et al., 2016; Foltz & McPhaden, 2010) or remotely generated by the radiation of Rossby waves from coastal trapped waves generated by local wind anomalies in the Gulf of Guinea (Chu et al., 2007). However, in a composite analysis of sea level anomalies, we could not clearly identify a reflection of an equatorial Kelvin wave at the eastern boundary or a Rossby wave propagating from the eastern basin to 5°N, 23°W prior to any eastward flow event.

6. NEUC and Oxygen

The NEUC is thought to transport oxygen-rich water from the western boundary towards the generally poorly ventilated eastern tropical North Atlantic (Brandt et al., 2010; Stramma et al., 2008). The mean ship section indicates a local oxygen maximum which is associated with the NEUC and single ship sections often show maxima in the area of the NEUC (Figure 3). Here we will investigate if the strong eastward NEUC events are associated with an increased eastward oxygen transport using moored observations.

We calculated oxygen anomalies on isopycnals. First, a temporal mean oxygen profile as a function of density was calculated from the mooring time series. Next, for each time step, the oxygen anomaly was calculated with respect to the mean oxygen value of the respective density. Finally, we applied a second-order 30-day low-pass Butterworth filter to both, the transport and oxygen time series (Figure 3).

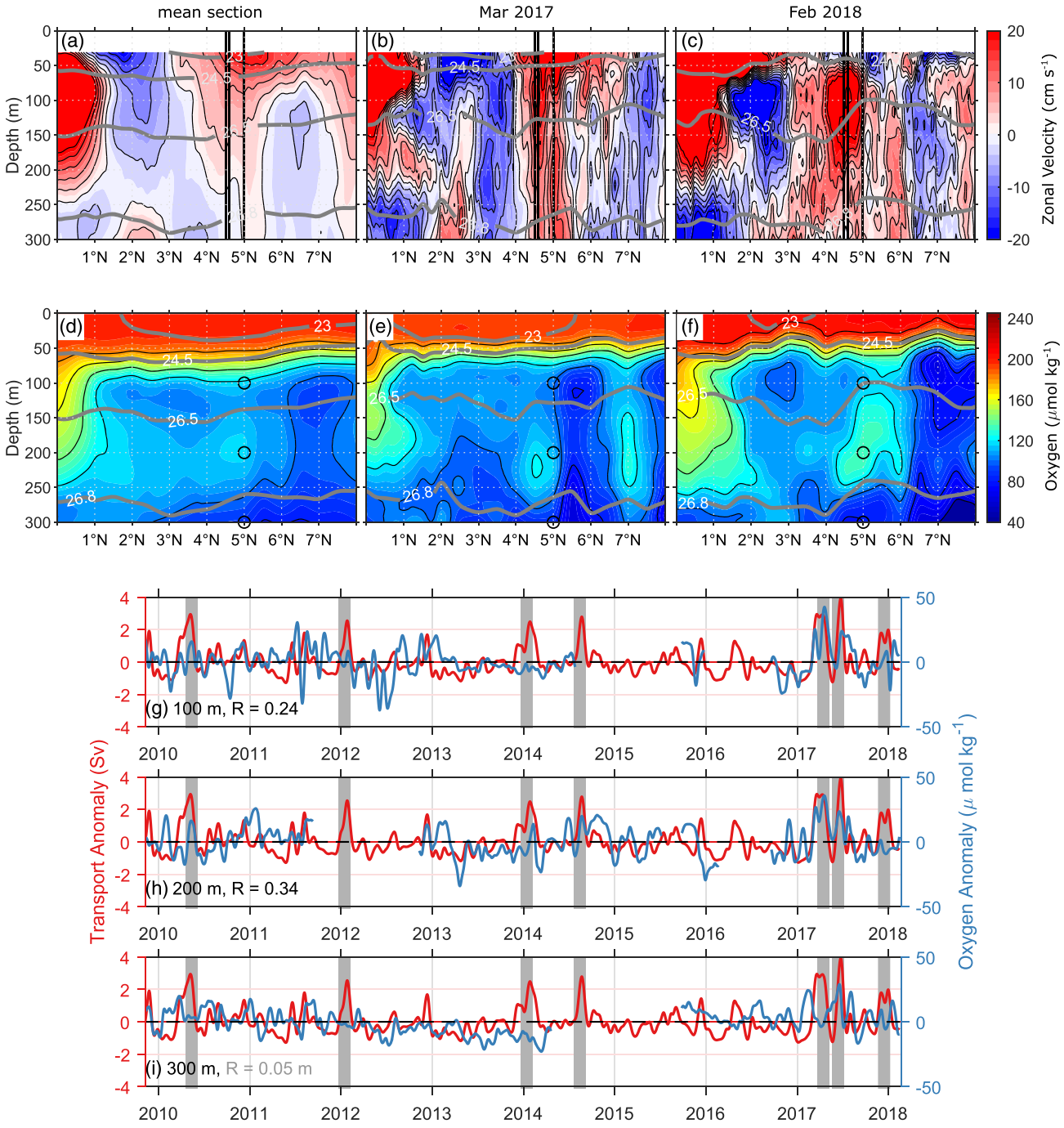

Figure 3. Zonal velocity (a–c) and oxygen (d–f) observations along 23°W with mean sections of all 24 cruises (a,d) and sections taken during Ronald H. Brown cruise PNE 2017 (b,e) and during Meteor cruise M145 (c,f). Grey lines mark neutral density surfaces (kg m^{-3}), black vertical lines (a–c) mark the position of moorings, black circles (d–f) mark single point oxygen measurements. (g–i) Thirty-day low-pass filtered NEUC tranport (red lines) and oxygen anomalies (blue lines) at 5°N, 23°W at a depth of (g) 100, (h) 200, and (i) 300 m. Grey bars mark strong NEUC events. *R* is the correlation coefficient of zonal velocity and oxygen anomalies at zero lag (black/grey color indicates that *R* is significant/not significant on a 95% confidence level).

In 100 and 200 m depth, we found a significant positive correlation between the NEUC transport and oxygen anomalies ($R_{\max,100\ m}$=0.35, NEUC leads by 16 days; $R_{\max,200\ m}$=0.35, NEUC leads by 2.5 days), while in 300 m depth, which is just below the NEUC, the correlation is not significant ($R_{300\ m}$=0.05, zero lag). If data are available, positive oxygen anomalies can be found during most of the strong eastward flow events except for

in 100 m depth during the 2012 and 2014 event. Year 2017 seems to be an exceptional year in the moored time series with the two strongest eastward flow events occurring consecutively within 6 months. Additionally, these two events are associated with some of the highest oxygen anomalies observed. The correlation between oxygen and NEUC transport anomalies during these two events is much higher compared to the rest of the time series. The correlation between the time series for the period from September 2016 to February 2018 is 0.63 (NEUC leads by 13.5 days) and 0.56 (NEUC leads by 1.5 days) in 100 and 200 m depth, respectively.

Positive oxygen anomalies also occur independently from strong eastward flow events and may be associated with changes in the meridional velocity. On intraseasonal timescales, zonal and meridional velocity anomalies are of similar strength and the dominant frequency band of the meridional velocity (30 to 70 days) overlaps with the frequency of the strong eastward flow events (1 to 5 months). It is thus not possible to clearly differentiate between the effect of meridional and zonal velocity on oxygen values at the mooring position. Yet we find no significant correlation between the 30-day low-pass filtered meridional velocity and oxygen anomalies ($-0.12 \leq R \leq 0.06$ at zero lag; supporting information, Figure S7).

7. Summary and Discussion

The NEUC is an eastward flowing current centered around 5°N in the tropical Atlantic. Although its core velocity is weak (below 0.3 m s^{-1}) it is thought to act as an important oxygen supply route towards the eastern tropical North Atlantic oxygen minimum zone (Brandt et al., 2010; Stramma et al., 2008). For the first time, we reconstructed a time series of the NEUC transport based purely on direct velocity observations. By combining moored zonal velocities at 5°N, 23°W and meridional ship sections along ~23°W we obtained a NEUC transport time series from June 2006 to February 2008 and November 2009 to January 2018. In contrast to previous studies (Burmeister et al., 2019; Goes et al., 2013; Hüttl-Kabus & Böning, 2008), neither the moored zonal velocity at 5°N (Figure 1) nor the reconstructed eastward NEUC transport (Figure 2) exhibits a pronounced seasonal cycle. We find that both time series are dominated by strong intraseasonal eastward flow events which can peak throughout the year (Figures 1 and 2). Although in the mean meridional ship sections the zonal velocity maximum associated with the NEUC coincides with a local oxygen maximum, we find that the eastward flow events are only occasionally associated with high oxygen levels (Figure 3).

We reconstructed the NEUC transport at 23°W based on velocity observations from three moorings and 24 meridional ship sections (Figure 2). To obtain a longer time series, we then reconstructed the NEUC variability based on data from only one mooring position. The comparison with the three-mooring solution indicates that the variability is dominated by a meridionally homogeneous structure covering the complete integration box (Figure S3). However, the method has some limitations. The used integration box does not cover the entire NEUC region (Figure S1). Consequently, our method is underestimating the true NEUC transport. A comparison of the box integrated transport calculated from ship sections with a reference transport calculated from ship sections using a path following algorithm indicates that the box integrated transport represents the variability of the NEUC reasonably well (R=0.9, Figures S2 and S5). An additional uncertainty of the reconstructed transport is due to the upper range of the moored velocity observations that varies between 65 and 85 m, that is, the moored observations do not always cover the entire NEUC depth range. In summary, the used method is underestimating the true NEUC strength, but it is still capable of representing its variability, as this is dominated by a homogeneous structure in latitude and depth.

Within the scope of this paper, we could not identify a clear forcing mechanism for the strong eastward flow events. We found that easterly wind stress anomalies in the eastern equatorial basin are leading the NEUC transport by 1 to 2 months. Zonal wind stress anomalies and associated wind stress curl anomalies could directly (Burmeister et al., 2016; Foltz & McPhaden, 2010) or remotely (Chu et al., 2007) force Rossby waves which reach 5°N, 23°W to cause the observed eastward flow events. However, we could not clearly identify a Rossby wave propagating from the eastern basin to 5°N, 23°W prior to any event. Other potential mechanisms might include nonlinear processes resulting, for example, in the development of multiple cores that were discussed by Furue et al. (2007). These cores that were superimposed on the otherwise linear arrested front dynamics (Dewar, 1991) were identified in simulations with enhanced horizontal resolution.

Finally, we investigated the relationship between the NEUC transport events and oxygen. In 2017, eastward transport and oxygen anomalies agree very well. For other events, the correlation is weaker or non-existent

(Figure 3). One possible explanation is that the local oxygen maximum associated with the NEUC is not located directly at 5°N as visible in the meridional ship sections of March 2017 (Figures 3b and 3e). In that case, the higher oxygen concentrations are simply not captured by the mooring. Another explanation may be that some strong eastward flow events are not connected to the well-ventilated western boundary but are instead supplied out of the westward flow of low-oxgen waters north and south of the NEUC. For example, in the meridional section of February 2018, we find strong eastward velocities between 4°N and 5°N at 50 and 100 m depth that are associated with low oxygen concentrations, which might be due to a recirculation of low-oxygen waters typically present south of the NEUC (Figures 3c and 3f Burmeister et al., 2019). As the zonal velocity events with a duration between 1 and 5 months overlap with the dominant frequency band of meridional velocity (30 to 70 days), it is not possible to clearly differentiate between the effect of meridional and zonal velocity on oxygen. However, we did not find any correlation between the meridional velocity and oxygen anomalies on intraseasonal time scales at 5°N, 23°W. Furthermore, Hahn et al. (2014) found that the mean meridional eddy flux at the mooring position is not significantly different from zero. Consistent with previous studies (Burmeister et al., 2019; Hahn et al., 2014; Weisberg & Weingartner, 1988), we suggest that a continuous flow of oxygen-rich water from the western boundary toward the eastern Atlantic basin by the NEUC is regularly altered by TIWs or other mesoscale recirculations. This can explain why not all NEUC transport events are associated with higher oxygen levels. Nevertheless, the significant positive correlation between the 30-day low-pass filtered NEUC transport and oxygen anomalies at 5°N, 23°N (Figure 3) indicates that the NEUC transport events likely result in an elevated mean eastward oxygen transport and contribute to the oxygen maximum observed in ship sections at the NEUC core position.

Acknowledgments

This study was funded by the Deutsche Forschungsgemeinschaft as part of the Sonderforschungsbereich 754 Climate-Biogeochemistry Interactions in the Tropical Ocean, through several research cruises with RV L'Atalante, RV Maria S. Merian, RV Meteor, and RV Polarstern, by the project FOR1740 and by the Deutsche Bundesministerium für Bildung und Forschung (BMBF) as part of projects RACE (03F0651B) and RACE-Synthesis (03F0824C). This project has received funding from the European Unions Horizon 2020 research and innovation programme under grant agreement No 818123 (iAtlantic) and grant agreement No 817578 (TRIATLAS). This output reflects only the authors view and the European Union cannot be held responsible for any use that may be made of the information contained therein. We thank the captains, crews, scientists, and technical groups involved in the different national and international research cruises to the eastern tropical North Atlantic that contributed to collecting CTD, velocity as well as mooring data, and making them freely available. We thank Rebecca Hummels for post-processing of the recent mooring and ship section data. The shipboard data are accessible at https://doi.pangaea.de/10.1594/PANGAEA.899052. The mooring data are accessible at https://doi.pangaea.de/10.1594/PANGAEA.903913. We are grateful to NOAA/PMEL and NOAA/AOML for making the data of the PIRATA Northeast Extension cruises freely available at https://www.aoml.noaa.gov/phod/pne/cruises.php. ASCAT data were obtained from the Centre de Recherche et d'Exploitation Satellitaire (CERSAT), at IFREMER, Plouzan (France) and are available at ftp://ftp.ifremer.fr/ifremer/cersat/products/gridded/MWF/L3/ASCAT/Daily/. Global Ocean Gridded L4 sea surface heights and derived variables were made available by E.U. Copernicus Marine Environment Monitoring Service (CMEMS). Data are available at https://marine.copernicus.eu/services-portfolio/access-to-products/?option=com_csw&view=details&product_id=SEALEVEL_GLO_PHY_L4_REP_OBSERVATIONS_008_047. The JRA-55 reanalysis surface winds used for this study are provided by the Japanese 55-year Reanalysis (JRA-55) project carried out by the Japan Meteorological Agency (JMA) and are available at https://jra.kishou.go.jp/JRA-55/index_en.html#jra-55 after registration.

References

Bentamy, A., & Fillon, D. C. (2012). Gridded surface wind fields from Metop/ASCAT measurements. *International Journal of Remote Sensing*, *33*(6), 1729–1754. https://doi.org/10.1080/01431161.2011.600348

Bourlès, B., D'Orgeville, M., Eldin, G., Gouriou, Y., Chuchla, R., DuPenhoat, Y., & Arnault, S. (2002). On the evolution of the thermocline and subthermocline eastward currents in the Equatorial Atlantic. *Geophysical Research Letters*, *29*(16), 43. https://doi.org/10.1029/2002GL015098

Bourlès, B., Gouriou, Y., & Chuchla, R. (1999). On the circulation in the upper layer of the western equatorial Atlantic. *Journal of Geophysical Research*, *104*(C9), 21,151–21,170. https://doi.org/10.1029/1999JC900058

Brandt, P., Bange, H. W., Banyte, D., Dengler, M., Didwischus, S. H., Fischer, T., et al. (2015). On the role of circulation and mixing in the ventilation of oxygen minimum zones with a focus on the eastern tropical North Atlantic. *Biogeosciences*, *12*(2), 489–512. https://doi.org/10.5194/bg-12-489-2015

Brandt, P., Funk, A., Tantet, A., Johns, W. E., & Fischer, J. (2014). The equatorial undercurrent in the central Atlantic and its relation to tropical Atlantic variability. *Climate Dynamics*, *43*(11), 2985–2997. https://doi.org/10.1007/s00382-014-2061-4

Brandt, P., Hormann, V., Körtzinger, A., Visbeck, M., Krahmann, G., Stramma, L., & Schmid, C. (2010). Changes in the ventilation of the oxygen minimum zone of the Tropical North Atlantic. *Journal of Physical Oceanography*, *40*(8), 1784–1801. https://doi.org/10.1175/2010JPO4301.1

Burmeister, K., Lübbecke, J. F., & Brandt, P. (2016). Revisiting the cause of the eastern equatorial Atlantic cold event in 2009. *Journal of Geophysical Research: Ocean*, *7*, 4777–4789. https://doi.org/10.1002/2016JC011719

Burmeister, K., Lübbecke, J. F., Brandt, P., & Duteil, O. (2019). Interannual variability of the Atlantic North Equatorial Undercurrent and its impact on oxygen. *Journal of Geophysical Research: Ocean*, *124*, 2348–2373. https://doi.org/10.1029/2018JC014760

Chu, P. C., Ivanov, L. M., Melnichenko, O. V., & Wells, N. C. (2007). On long baroclinic Rossby waves in the tropical North Atlantic observed from profiling floats. *Journal of Geophysical Research*, *112*, C05032. https://doi.org/10.1029/2006JC003698

Dewar, W. K. (1991). Arrested fronts. *Journal of Marine Research*, *49*, 21–52. https://doi.org/10.1357/002224091784968576

Fischer, J., Brandt, P., Dengler, M., Müller, M., & Symonds, D. (2003). Surveying the upper ocean with the ocean surveyor: A new phased array Doppler current profiler. *Journal of Atmospheric and Oceanic Technology*, *20*(5), 742–751. https://doi.org/10.1175/1520-0426(2003)20<742:STUOWT>2.0.CO;2

Foltz, G. R., & McPhaden, M. J. (2010). Interaction between the Atlantic meridional and Niño modes. *Journal of Geophysical Research*, *37*, L18604. https://doi.org/10.1029/2010GL044001

Furue, R., McCreary, Jr. J. P., & Yu, Z. (2009). Dynamics of the Northern Tsuchiya Jet*. *Journal of Physical Oceanography*, *39*(9), 2024–2051. https://doi.org/10.1175/2009JPO4065.1

Furue, R., McCreary, Jr. J. P., Yu, Z., & Wang, D. (2007). Dynamics of the Southern Tsuchiya Jet*. *Journal of Physical Oceanography*, *37*(3), 531–553. https://doi.org/10.1175/JPO3024.1

Goes, M., Goni, G., Hormann, V., & Perez, R. C. (2013). Variability of the Atlantic off-equatorial eastward currents during 1993-2010 using a synthetic method. *Journal of Geophysical Research: Ocean*, *118*, 3026–3045. https://doi.org/10.1002/jgrc.20186

Hüttl-Kabus, S., & Böning, C. W. (2008). Pathways and variability of the off-equatorial undercurrents in the Atlantic Ocean. *Journal of Geophysical Research*, *113*, C10018. https://doi.org/10.1029/2007JC004700

Hahn, J., Brandt, P., Greatbatch, R. J., Krahmann, G., & Körtzinger, A. (2014). Oxygen variance and meridional oxygen supply in the Tropical North East Atlantic oxygen minimum zone. *Climate Dynamics*, *43*(11), 2999–3024. https://doi.org/10.1007/s00382-014-2065-0

Hahn, J., Brandt, P., Schmidtko, S., & Krahmann, G. (2017). Decadal oxygen change in the eastern tropical North Atlantic. *Ocean Science*, *13*(4), 551–576. https://doi.org/10.5194/os-13-551-2017

Hazeleger, W., & Drijfhout, S. (2006). Subtropical cells and meridional overturning circulation pathways in the tropical Atlantic. *Journal of Geophysical Research*, *111*, C03013. https://doi.org/10.1029/2005JC002942

Hsin, Y. C., & Qiu, B. (2012). Seasonal fluctuations of the surface North Equatorial Countercurrent (NECC) across the Pacific basin. *Journal of Geophysical Research*, *117*, C06001. https://doi.org/10.1029/2011JC007794

Jochum, M., & Malanotte-Rizzoli, P. (2003). On the generation of North Brazil Current rings. *Journal of Marine Research*, *61*(2), 147–173. https://doi.org/10.1357/002224003322005050

Jochum, M., & Malanotte-Rizzoli, P. (2004). A new theory for the generation of the equatorial subsurface countercurrents. *Journal of Physical Oceanography*, *34*(4), 755–771. https://doi.org/10.1175/1520-0485(2004)034<0755:ANTFTG>2.0.CO;2

Kobayashi, S., Ota, Y., Harada, Y., Ebita, A., Ota, Y., Moriya, M., et al. (2015). The JRA-55 reanalysis: General specifications and basic characteristics. *Journal of the Meteorological Society of Japan*, *93*(1), 5–48. https://doi.org/10.2151/jmsj.2015-001

Large, W. G., & Yeager, S. (2004). Diurnal to decadal global forcing for ocean and sea-ice models: The data sets and flux climatologies. *NCAR Technical Note NCAR/TN-460+STR*. https://doi.org/10.5065/D6KK98Q6

Marin, F., Hua, B. L., & Wacongne, S. (2000). The equatorial thermostad and subsurface countercurrents in the light of the dynamics of atmospheric Hadley cells. *Journal of Marine Research*, *58*(3), 405–437. https://doi.org/10.1357/002224000321511098

McCreary, Jr. J. P., Lu, P., & Yu, Z. (2002). Dynamics of the Pacific subsurface countercurrents. *Journal of Physical Oceanography*, *32*, 2379–2404. https://doi.org/10.1175/1520-0485(2002)032<2379:DOTPSC>2.0.CO;2

Schott, F. A., Dengler, M., Brandt, P., Affler, K., Fischer, J., Bourlès, B., & Rhein, M. (2003). The zonal currents and transports at 35 W in the tropical Atlantic. *Geophysical Research Letters*, *30*(7), 1349. https://doi.org/10.1029/2002GL016849

Schott, F. A., McCreary, Jr. J. P., & Johnson, G. C. (2004). Shallow overturning circulations of the tropical-subtropical oceans. *Earth's Climate*, *147*, 261–304.

Schott, F. A., Stramma, L., & Fischer, J. (1995). The warm water inflow into the western tropical Atlantic boundary regime, spring 1994. *Journal of Geophysical Research*, *100*(C12), 24,745–24,760. https://doi.org/10.1029/95JC02803

Stramma, L., Brandt, P., Schafstall, J., Schott, F., Fischer, J., & Körtzinger, A. (2008). Oxygen minimum zone in the North Atlantic south and east of the Cape Verde Islands. *Journal of Geophysical Research*, *113*, C04014. https://doi.org/10.1029/2007JC004369

Stramma, L., Prince, E. D., Schmidtko, S., Luo, J., Hoolihan, J. P., Visbek, M., et al. (2012). Expansion of oxygen minimum zones may reduce available habitat for tropical pelagic fishes. *Nature Climate Change*, *2*(1), 33–37. https://doi.org/10.1038/nclimate1304

Urbano, D. F., De Almeida, R. A., & Nobre, P. (2008). Equatorial undercurrent and north equatorial countercurrent at 38°W: A new perspective from direct velocity data. *Journal of Geophysical Research*, *113*, C04041. https://doi.org/10.1029/2007JC004215

Weisberg, R. H., & Weingartner, T. J. (1988). Instability waves in the Equatorial Atlantic Ocean. *Journal of Physical Oceanography*, *18*(11), 1641–1657. https://doi.org/10.1175/1520-0485(1988)018<1641:IWITEA>2.0.CO;2